

Supporting Information

Defective Nickel Sulfide Hierarchical Structure for Efficient Electrochemical Conversion of Plastic Waste to Value-Added Chemicals and Hydrogen Fuel

Zhijie Chen,^a Wei Wei,^a Yansong Shen,^b Bing-Jie Ni^{a,*}

^a Centre for Technology in Water and Wastewater, School of Civil and Environmental Engineering, University of Technology Sydney, Sydney, NSW 2007, Australia

^b School of Chemical Engineering, University of New South Wales, Sydney, NSW 2052, Australia

***Corresponding Author:**

Prof Bing-Jie Ni

E-mail: bingjieni@gmail.com

Experimental

Chemicals and materials

Thiourea ($\text{CH}_4\text{N}_2\text{S}$), cobalt nitrate hexahydrate ($\text{Co}(\text{NO}_3)_2 \cdot 6\text{H}_2\text{O}$), sodium borohydride (NaBH_4), ethanol ($\text{C}_2\text{H}_6\text{O}$), ethylene glycol ($\text{C}_2\text{H}_6\text{O}_2$), potassium hydroxide (KOH), and concentrated sulfuric acid (H_2SO_4) were purchased from Fisher Scientific. Nickel foam (NF) was bought from Phychemi Hong Kong Company Limited. The 5% Nafion solution, commercial 20% Pt/C and RuO_2 catalysts, and anion exchange membrane were provided by Sigma-Aldrich Corporation. All the reagents were employed as obtained without further purification and distilled (DI) water utilized throughout all experiments was from a Millipore system.

Material characterizations

The crystal structure of materials was determined by X-ray diffraction (XRD) measurements on a Rigaku Smart-Lab 9 kW diffractometer with the X-ray tube operated at 45 kV and 20 mA. The morphology of catalysts was recorded with scanning electron microscopy (SEM, Zeiss Sigma 500). The Raman spectra were tested on a ThermoFisher DXRi Raman microscope. Transmission electron microscopy (TEM) and high-resolution TEM (HRTEM) images were obtained on a TEM instrument (FEI Tecnai G2 F20 S-TWIN) with an acceleration voltage of 200 kV. Energy dispersive spectroscopy (EDS) mapping measurements were conducted by a TEM which is equipped with an EDS. The element composition and surface

chemistry of catalysts were tested by the X-ray photoelectron spectroscopy (XPS, Thermo K-Alpha⁺, Thermo Fisher Scientific, USA) with the Al (K_α) radiation. Electron paramagnetic resonance (EPR) signals were recorded by a (JEOL) JES FA200 spectrometer to investigate the sulfur vacancies. The ion concentrations in the electrolyte and element contents in catalysts were measured by an inductively coupled plasma mass spectrometry (ICP-MS) instrument (Agilent 7700s). ¹H and ¹³C nuclear magnetic resonance (NMR) spectroscopy was recorded on a 600 MHz/AVANCE 400 (Bruker).

Electrochemical tests

The oxygen evolution reaction (OER), ethylene glycol oxidation reaction (EGOR), and hydrogen evolution reaction (HER) performance of catalysts for was tested in a H-type cell, with a CHI 660E electrochemical workstation. The as-prepared NF-supported nickel sulfides were directly used as the working electrode. Hg/HgO serves as the reference electrode, and a graphite rod is the counter electrode. For the preparation of Pt/C and RuO₂ electrode, 5 mg of commercial catalyst powder was first dispersed in 1 mL of mixed solution (500 μL of water, 450 μL of ethanol, and 50 μL of 5 wt% Nafion solution). After sonication for about 30 min, a homogeneous ink was obtained. Then, 100 μL of the ink was deposited onto a piece of acid-treated nickel foam (NF). Linear sweep voltammetry (LSV) curves were recorded at a scan rate of 5 mV s⁻¹. To eliminate the contributions of oxidation current densities of metal species to OER and EGOR, LSV curves were recorded by sweeping from high to low

potentials. The polarization curves were calibrated with 90% iR compensation to eliminate the solution resistance. All potentials measured were converted to the reversible hydrogen electrode (RHE) via the following equation: $E_{\text{vs. RHE}} = E_{\text{vs. Hg/HgO}} + 0.059 \text{ pH} + 0.098 \text{ V}$. For the EGOR tests, electrochemical impedance spectroscopy (EIS) was recorded at 1.32 V vs. RHE over the frequency range of 10^{-2} to 10^5 Hz, with an AC signal amplitude of 5 mV. The double-layer capacitances (C_{dl}) were calculated by conducting CVs at different scan rates (i.e., 10, 20, 30, 40, and 50 mV s^{-1}). Furthermore, the value of ECSA was calculated by the equation: $\text{ECSA} = S * C_{\text{dl}} / C_s$, where C_{dl} is the double layer capacitance; C_s is the general specific capacitance, the value is about 0.04 mF cm^{-2} , and S is the area of the working electrode. To test the long-term stability of catalysts, the chronoamperometric i-t curves were measured for 24 h.

To study the Faradic efficiency (FE) and yield of formate at different potentials, the EGOR was carried out at the potentiostatic mode. After reactions, the concentration of substrate and products were analyzed by a nuclear magnetic resonance (NMR) spectrometer. ^1H and ^{13}C NMR spectra were recorded on a 600 MHz/AVANCE 400 (Bruker), in which 300 μL electrolyte was added with 300 μL D_2O and 30 μL dimethyl sulfoxide (DMSO) used as an internal standard. The Faradaic efficiency (FE), formate selectivity and yield were calculated with the following equations:

$$\text{FE (\%)} = 100\% \times \frac{N(\text{formate})}{\text{total charge passed}/(n \times 96485)}$$

$$\text{Formate selectivity (\%)} = 100\% \times \frac{N(\text{formate})}{2N(\text{converted EG})}$$

$$\text{Formate yield (mmol cm}^{-2} \text{ h}^{-1}\text{)} = \frac{N(\text{formate})}{\text{electrode area} \times \text{reaction time}}$$

where N represents the moles of substances, n is the number of electron transfer for each product formation.

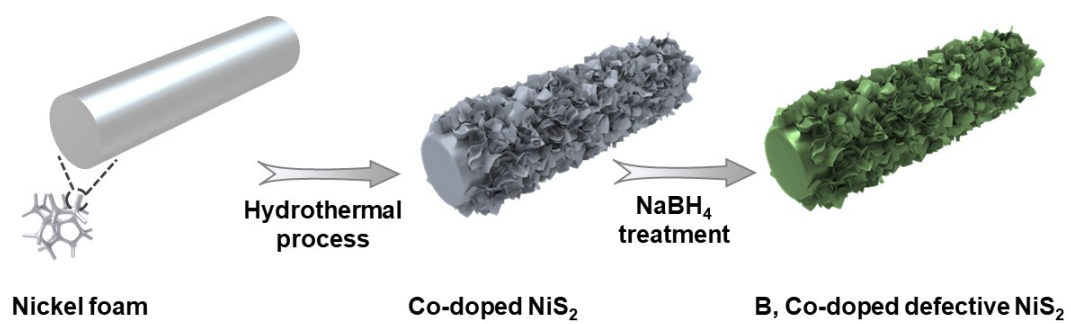


Figure S1. Scheme of the synthesis of B, Co co-doped defective NiS₂.

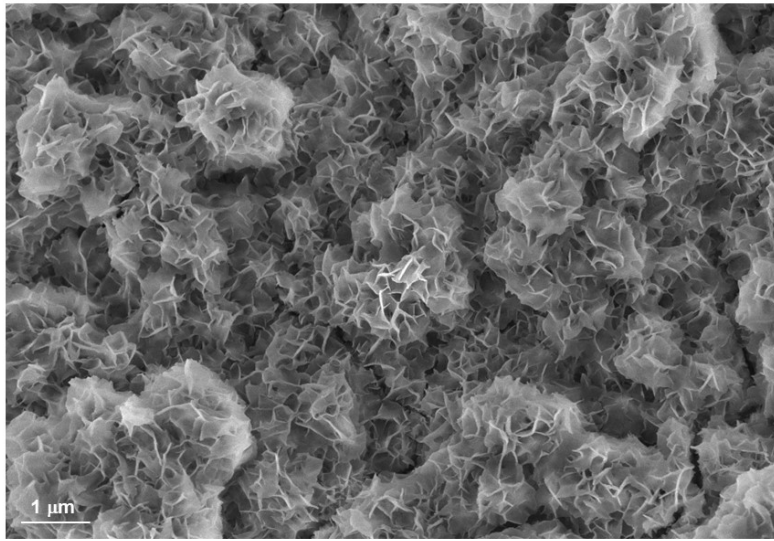


Figure S2. SEM image of B,Co-NiS.

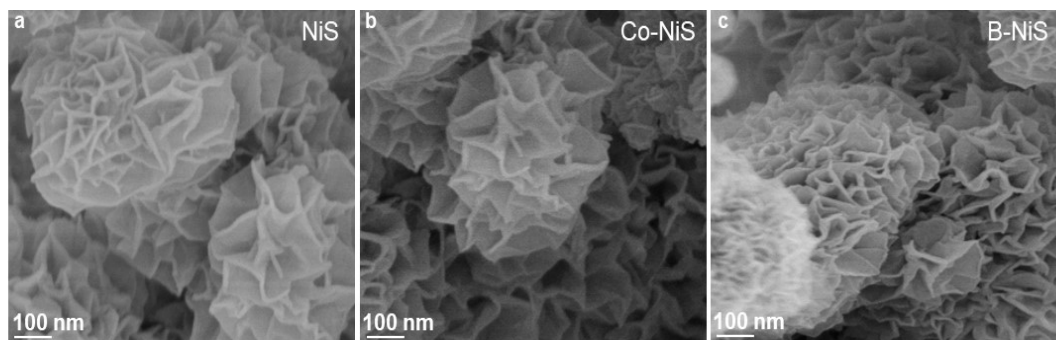


Figure S3. SEM images of (a) NiS, (b) Co-NiS, and (c) B-NiS.

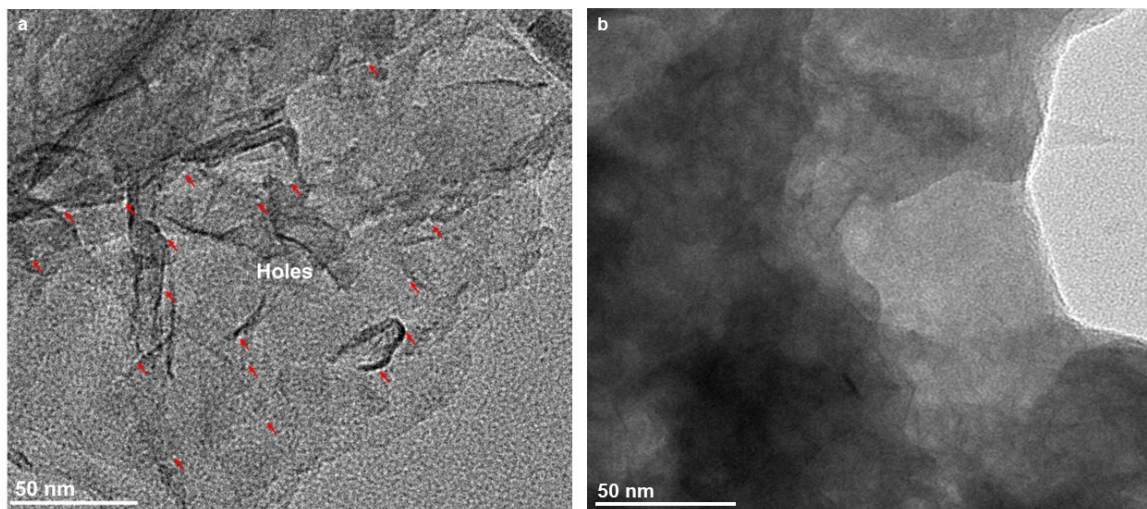


Figure S4. TEM images of (a) B,Co-NiS and (b) Co-NiS.

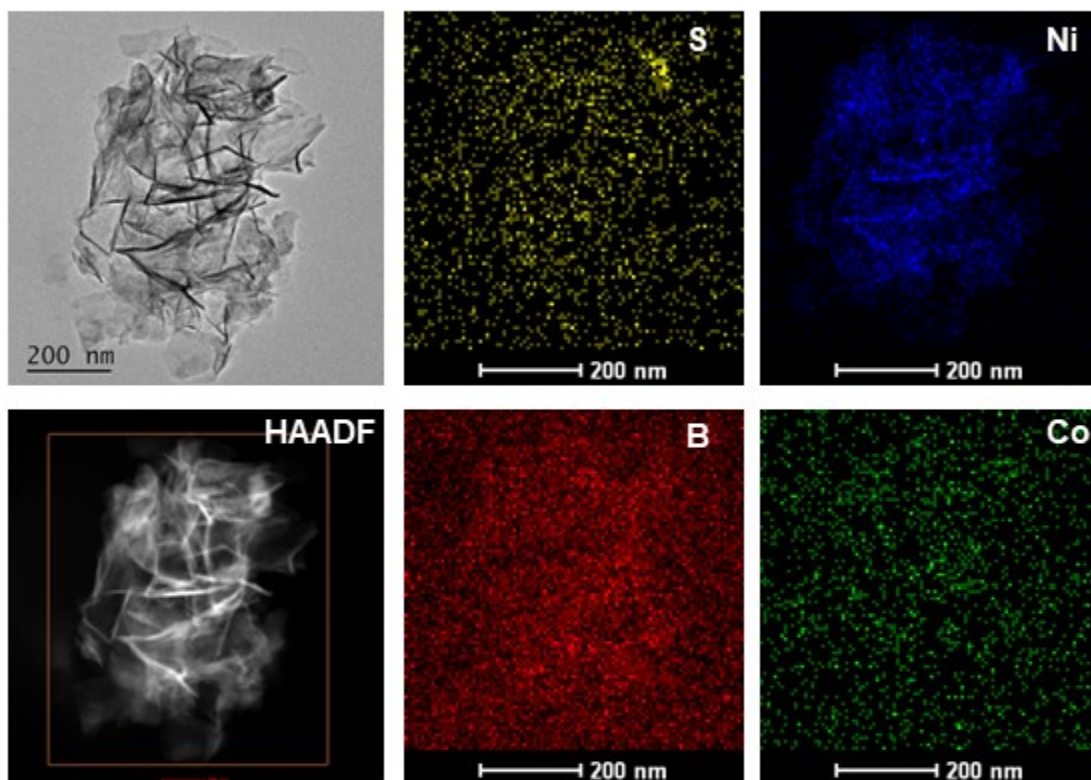


Figure S5. TEM image, HAADF-STEM image, and corresponding elemental mapping image of B,Co-NiS.

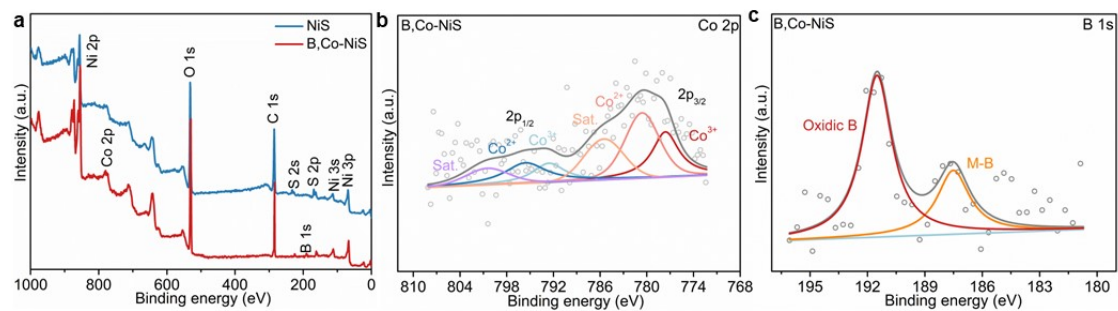


Figure S6. (a) XPS survey spectra of B,Co-NiS and NiS. High-resolution XPS spectra for (b) Co 2p and (c) B 1s of B,Co-NiS.

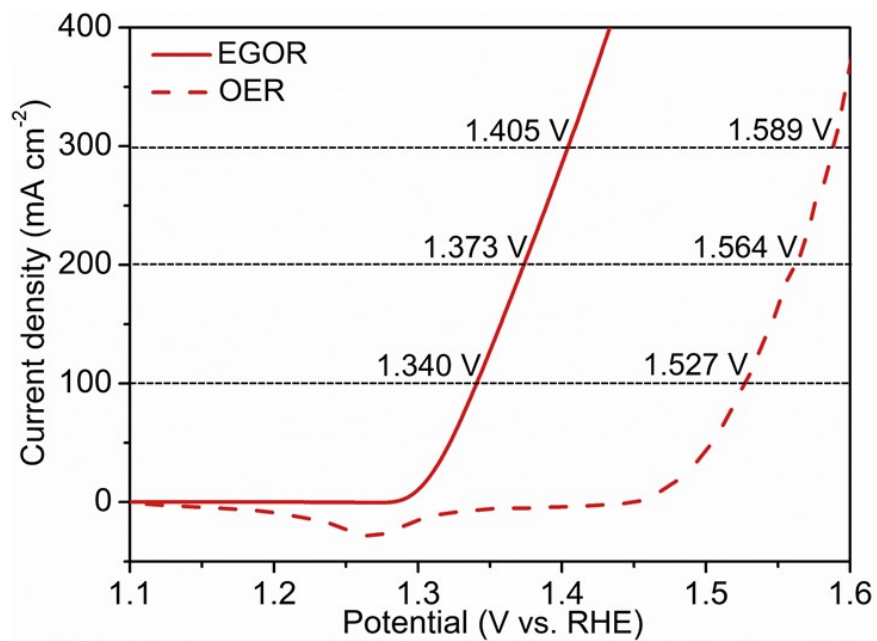


Figure S7. OER and EGOR LSV curves of B,Co-NiS.

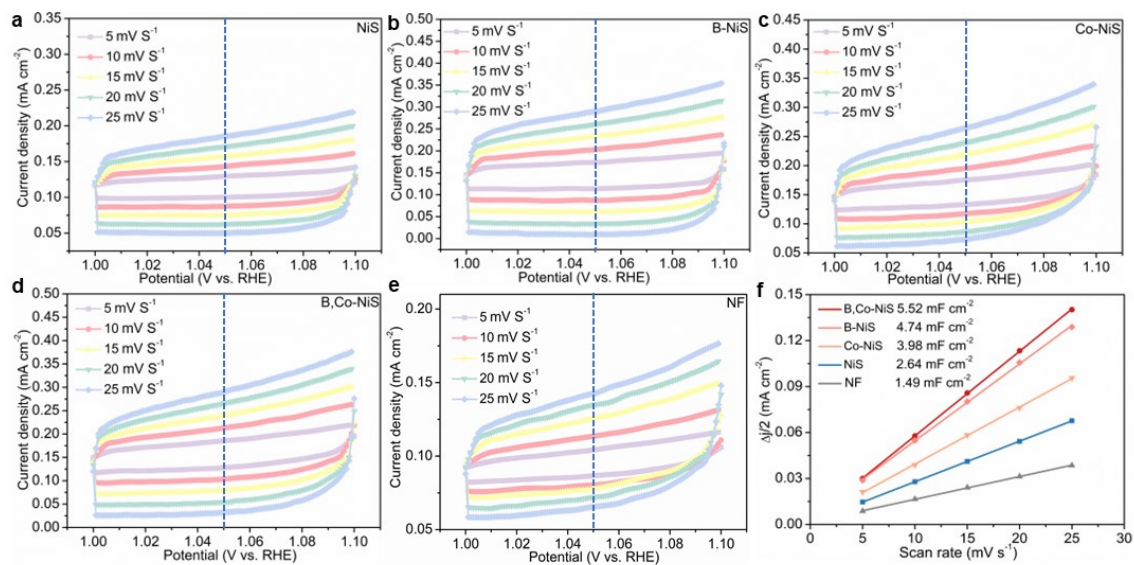


Figure S8. Cyclic voltammograms of (a) NiS, (b) B-NiS, (c) Co-NiS, (d) B,Co-NiS, and (e) NF at different scan rates (from 5 to 25 mV s⁻¹ with an increment of 5 mV s⁻¹). (f) The difference in current density ($\Delta j = (j_a - j_c)/2$) plots against the scan rate of NiS, B-NiS, Co-NiS, B,Co-NiS, and NF.

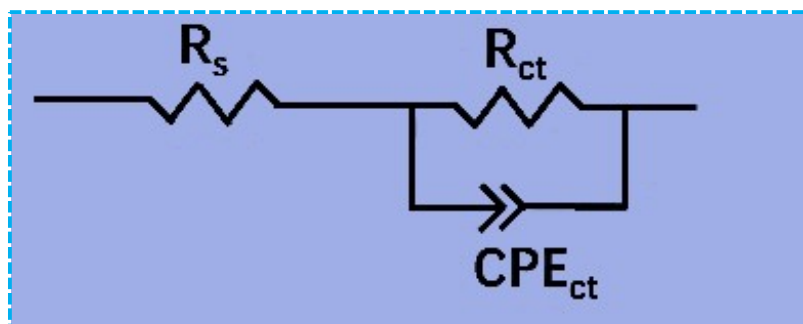


Figure S9. Equivalent circuit model for EIS data fitting.

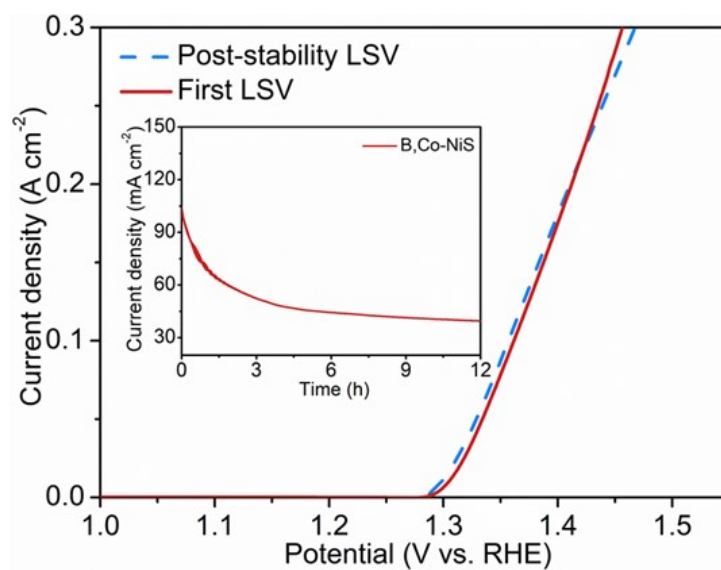


Figure S10. LSV curves of B,Co-NiS before and after 12 h EGOR test. Insert shows the chronoamperometric curve of B,Co-NiS for the 12 h EGOR test.

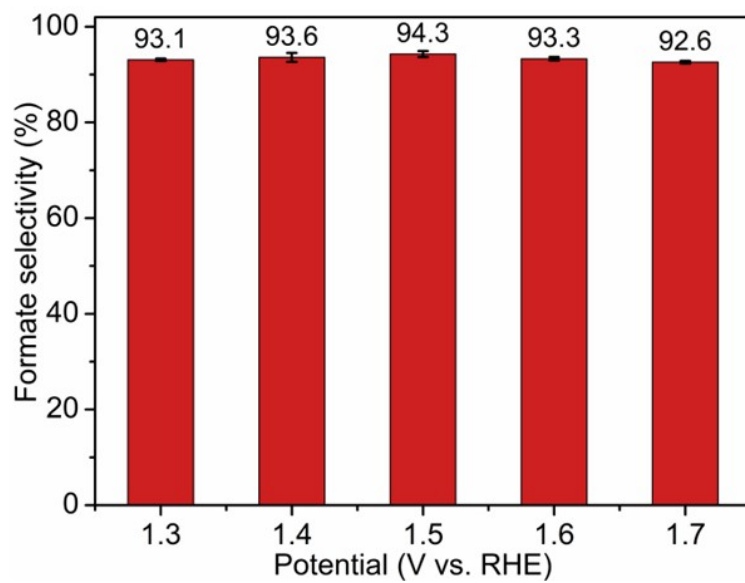


Figure S11. Formate selectivity of B,Co-NiS at varied applied voltages.

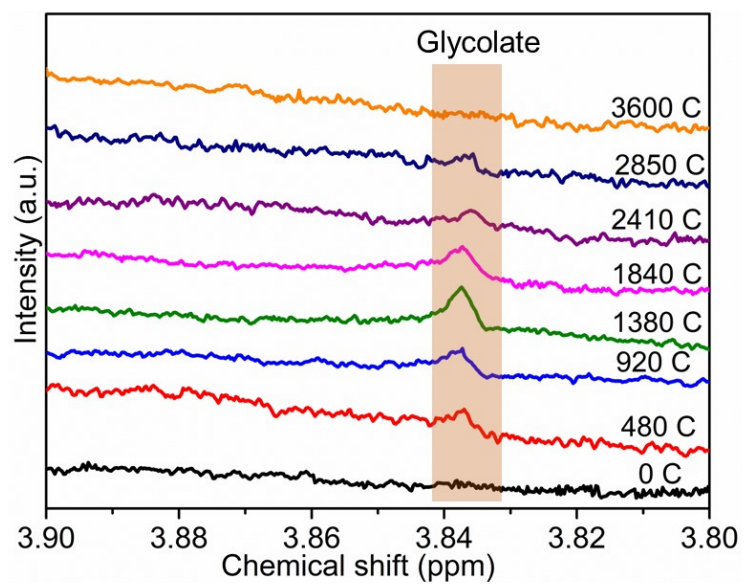


Figure S12. An enlarged part of the ^1H NMR spectra of products during EGOR process.

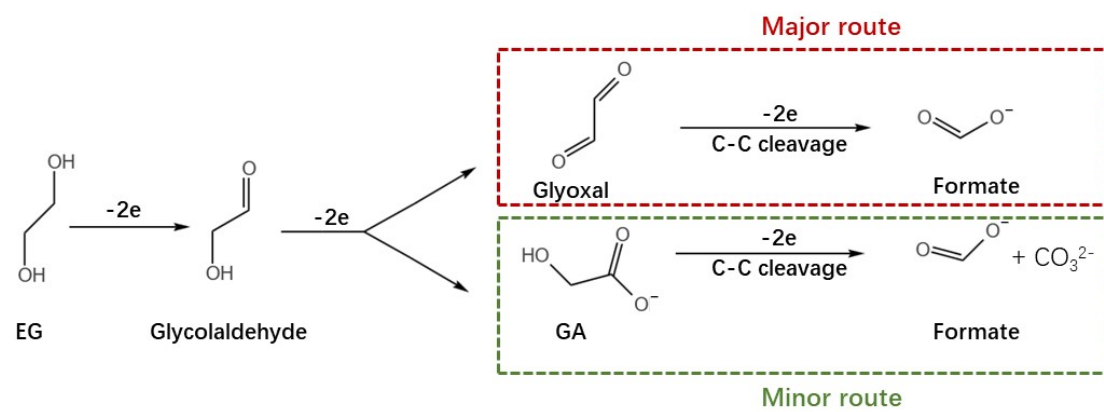


Figure S13. Proposed EGOR mechanism over the B₂Co-NiS catalyst.

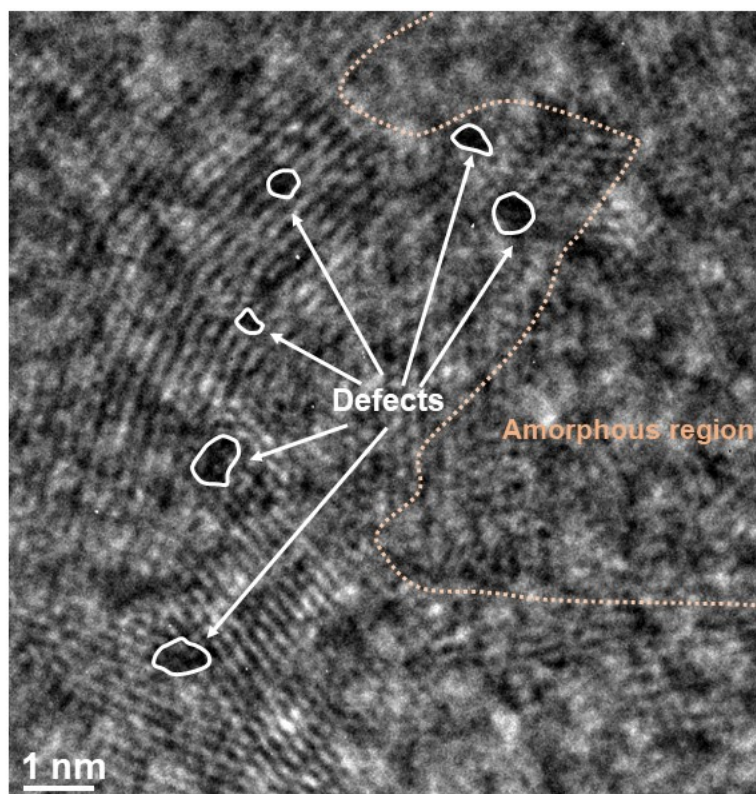


Figure S14. HRTEM image of post-EGOR B,Co-NiS.

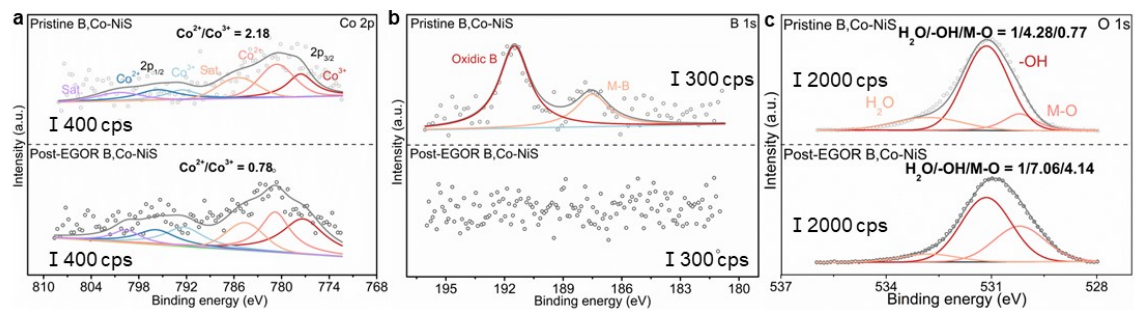


Figure S15. High-resolution XPS spectra for (a) Co 2p, (b) B 1s, and (c) O 1s of B,Co-NiS before and after the EGOR process.

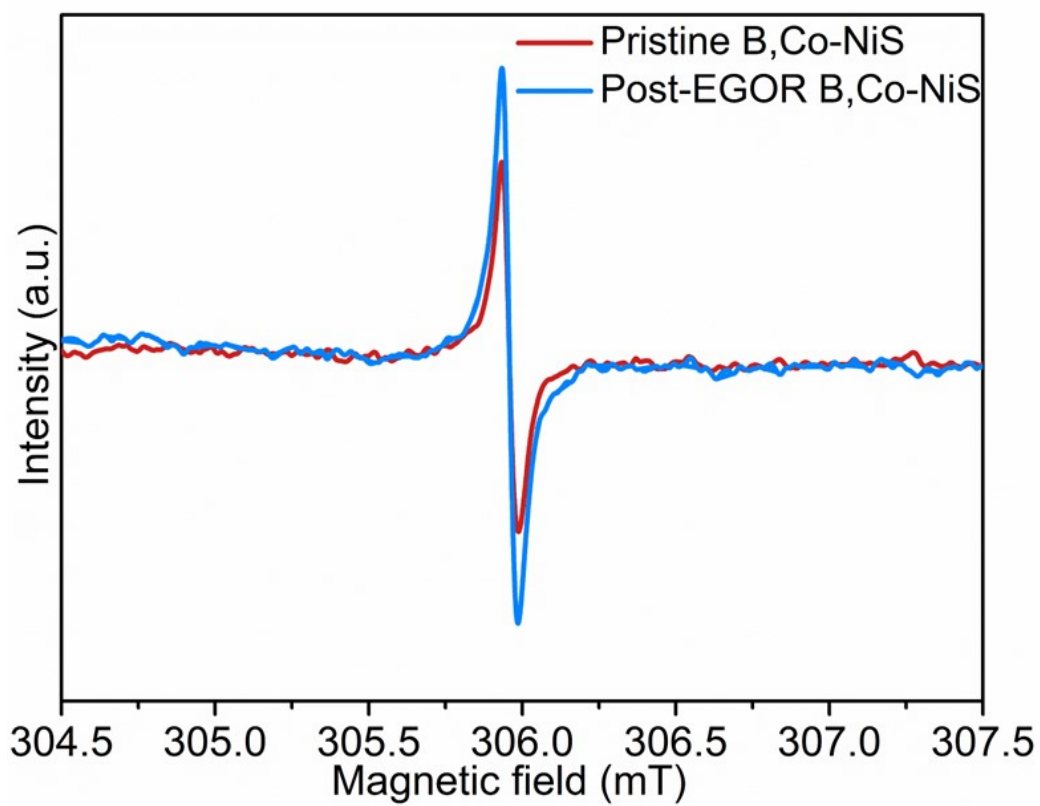


Figure S16. EPR spectra of B,Co-NiS before and after the EGOR test.

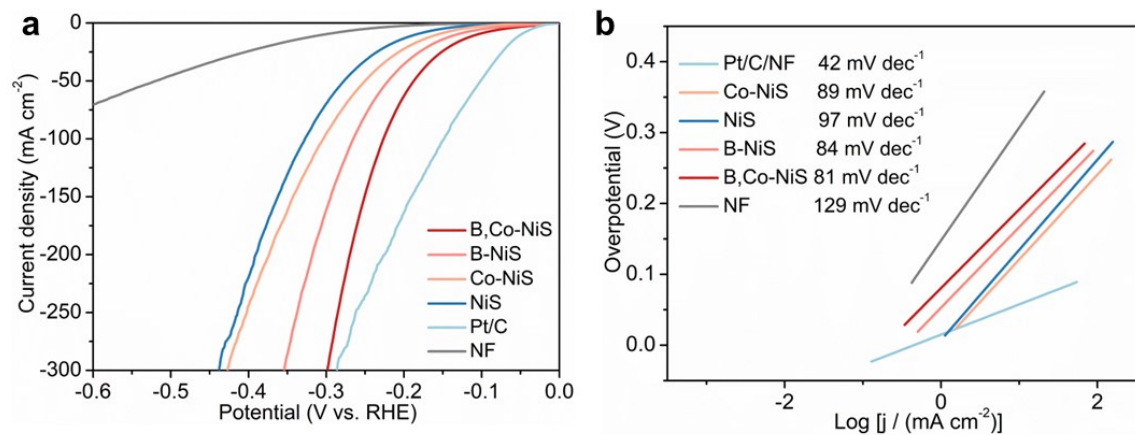


Figure S17. (a) LSV curves and (b) Tafel plots for HER of catalysts.

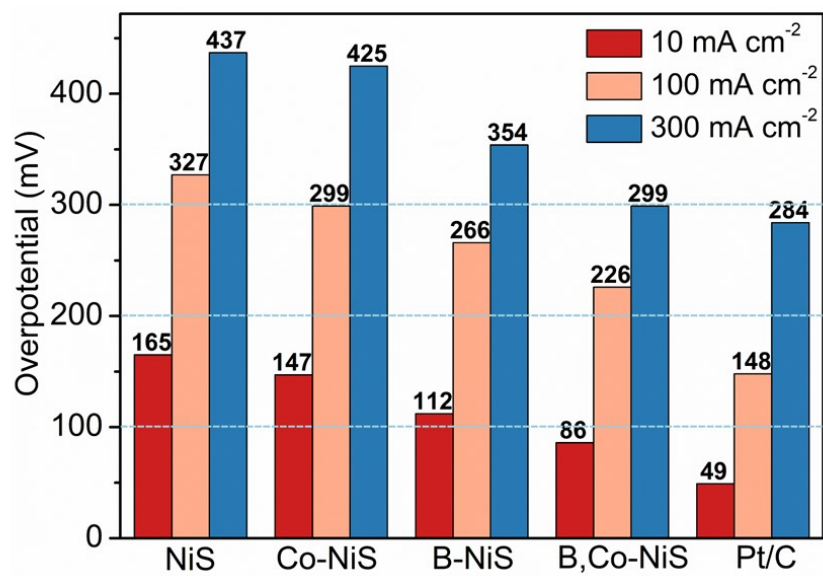


Figure S18. Comparison of HER overpotentials of catalysts at different current densities.

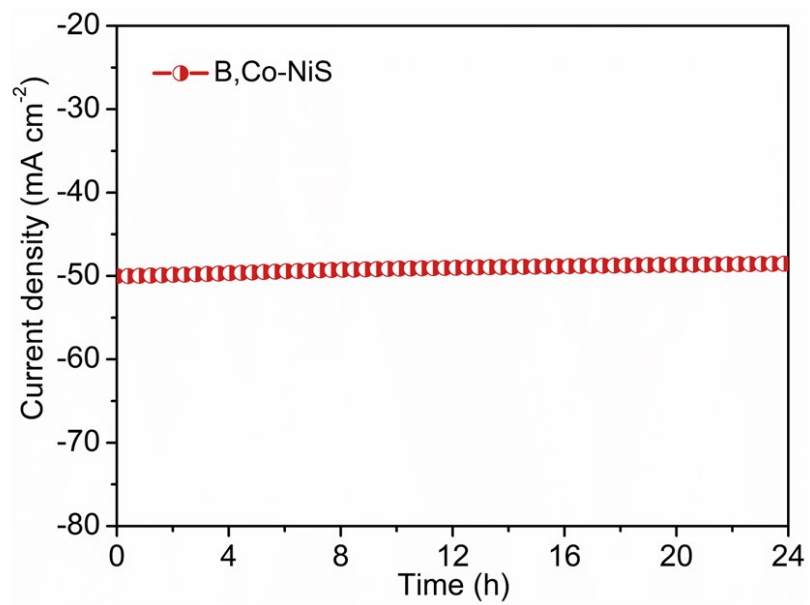


Figure S19. Chronoamperometric curve of B,Co-NiS for the 24 h HER test.

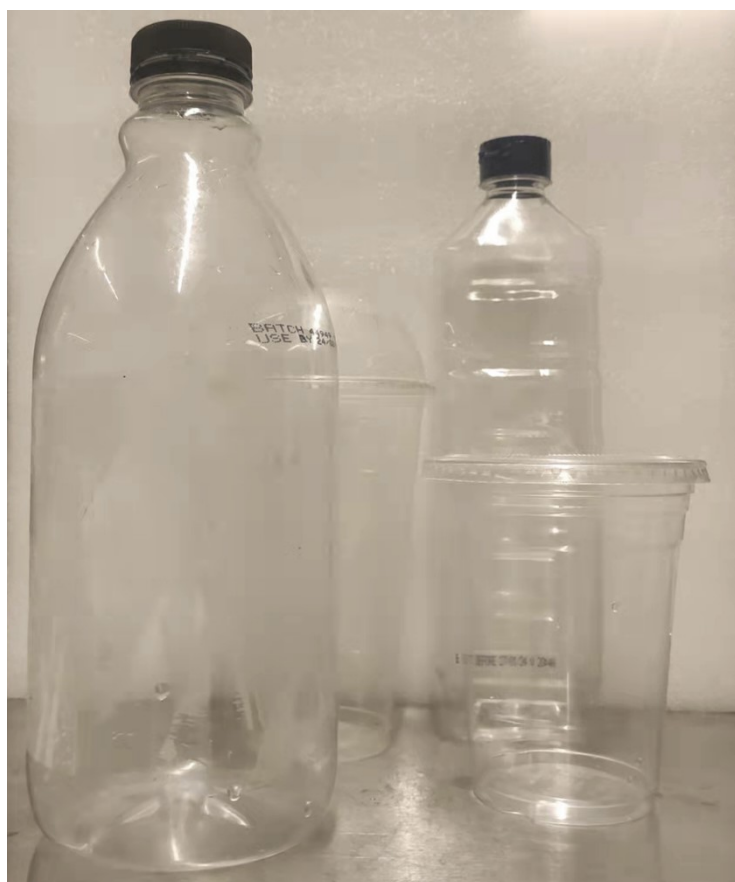


Figure S20. Picture of the collected PET waste.

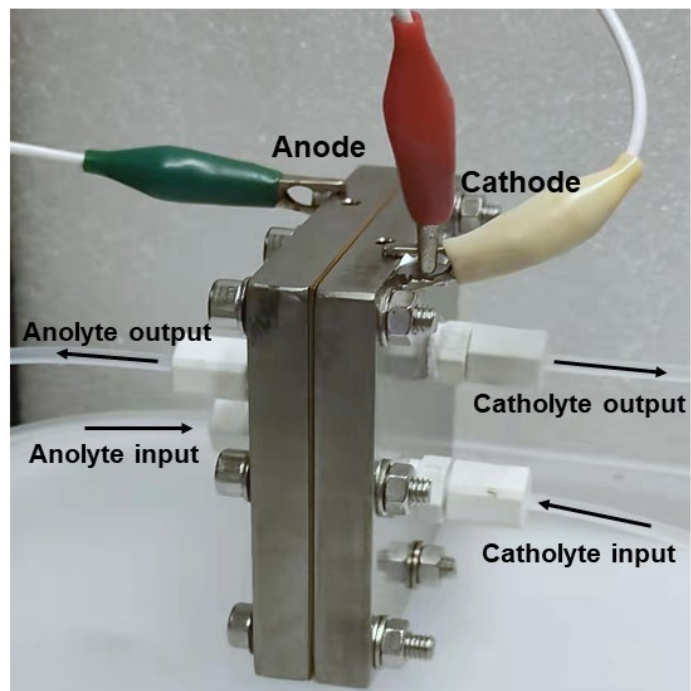


Figure S21. Photo of the home-made membrane-electrode assembly (MEA) flow electrolyzer.

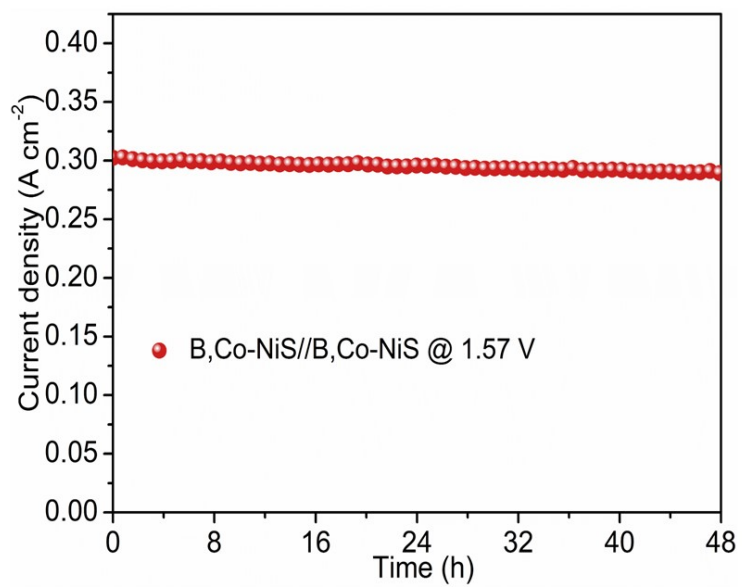


Figure S22. Stability test of the PET hydrolysate electrolyzer with B,Co-NiS as the bifunctional catalyst.

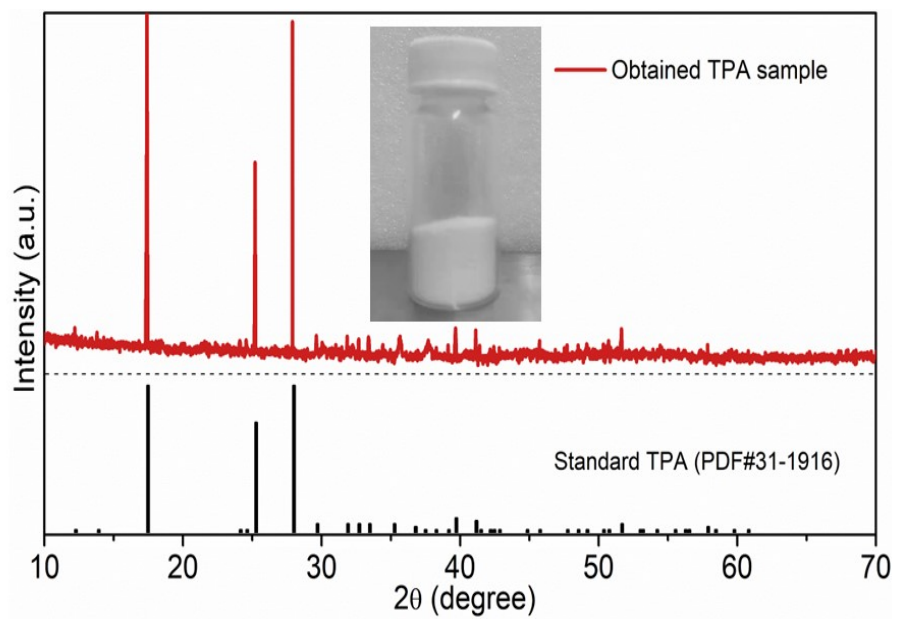


Figure S23. XRD pattern of the recovered TPA. Insert: picture of the recovered TPA.

Table S1. A summary of OER properties of B,Co-NiS and state-of-the-art electrocatalysts in 1 M KOH.

Catalyst	η_{10} (mV)	Reference
Mn ₃ N ₂	270	<i>Angew. Chem. Int. Ed.</i> 2018, 57, 698.
HG-NiFe	313	<i>Sci. Adv.</i> , 2018, 4, eaap7970.
Ni-NHGF	330	<i>Nat. Catal.</i> 2018, 1, 63.
CeO ₂ -CoS _{1.97}	264	<i>Adv. Mater.</i> 2021, 2102593.
Ni-MoN	276	<i>Adv. Energy Mater.</i> 2018, 8, 1802327.
S NiN _x -PC/EG	280	<i>Nat. Commun.</i> 2019, 10, 1392.
Fe-Mn-O NSs	273	<i>Adv. Funct. Mater.</i> 2018, 28, 1802463.
Co ₃ O ₄ /Co-Fe oxide	297	<i>Adv. Mater.</i> 2018, 30, 1801211.
Ni _{0.6} Co _{1.4} P	300	<i>Adv. Funct. Mater.</i> 2018, 28, 1706008.
NiMoO ₄ NRs-Fe-1	351	<i>J. Am. Chem. Soc.</i> 2021, 143, 14169-14177.
NiAs/GC	360	<i>Adv. Energy Mater.</i> 2019, 1900796
Fe-NiSe ₂ /GC	268	<i>Angew. Chem. Int. Ed.</i> 2018, 57, 4020-4024.
NiCeO _x /NF	295	<i>ACS Catal.</i> 2019, 9, 1605-1611.
NH ₄ CoPO ₄ ·H ₂ O	252	<i>Adv. Sci.</i> 2021, 2100498.
FeAs/NF	252	<i>Chem. Sci.</i> , 2020, 11, 11834.
Fe-doped Co ₃ O ₄	262	<i>Adv. Mater.</i> 2020, 2002235.
FeCoNiMo high-entropy alloy	250	<i>ACS Catal.</i> 2022, 12, 17, 10808–10817.
Co ₄ N@NC	257	<i>ACS Energy Lett.</i> 2020, 5, 692.
Co ₄ N/CNW/CC	310	<i>J. Am. Chem. Soc.</i> 2016, 138, 10226.
NiFe LDH NSA	269	<i>Nat. Commun.</i> 2018, 9, 2609.
Co _{0.5} (V _{0.5})	282	<i>Adv. Energy Mater.</i> 2020, 10, 1903571.
F-CoOOH/NF	270	<i>Angew. Chem. Int. Ed.</i> 2018, 57, 15471.
Co@N-CS/NHCP@CC	248	<i>Adv. Energy Mater.</i> 2019, 1803918.
3D Co(OH)F	313	<i>Adv. Mater.</i> 2017, 29, 1700286.
Fe-Co-P-O NBs	268	<i>Energy Environ. Sci.</i> 2019, 12, 3348.
SCFP-NF	310	<i>Adv. Mater.</i> 2018, 30, 1804333.
Ni _{0.75} Mn _{0.25} nanosheets	297	<i>ACS Energy Lett.</i> 2018, 3, 2150.

NiFeMn-LDH	262	<i>Energy Environ. Sci.</i> 2017, 10, 121–128.
CoFeZr oxides	248	<i>Adv. Mater.</i> 2019, 1901439.
B,Co-NiS	239	This study

Table S2. A summary of EGOR properties of B,Co-NiS and state-of-the-art electrocatalysts.

Catalyst	Current density (mA cm ⁻²)	Potential (V vs. RHE)	Electrolyte	Reference
NiCo ₂ O ₄ /CFP	50	1.44	1 M NaOH + 0.1 M EG	<i>ACS Catal.</i> 2022, 12, 11, 6722–6728.
CoNiB	10	1.31	1 M NaOH + 0.1 M EG	<i>J. Phys. Energy</i> 2023, 5, 024005.
Cobalt-Based Coordination Polymer	10	1.42	1 M KOH + 0.1 M EG	<i>ACS Catal.</i> 2023, 13, 1, 469–474.
Ni/WC@C	197	1.62	1 M NaOH + 1 M EG	<i>Chem. Mater.</i> 2022, 34, 3, 959–969.
OMS-Ni ₁ -CoP	50	1.38	1 M KOH + 0.5 M EG	<i>Appl. Catal. B</i> 2022, 316, 121667.
CuO	10	1.38	PET hydrolysate	<i>J. Phys. Chem. Lett.</i> 2022, 13, 2, 622–627
Ni ₃ N/W ₅ N ₄	10	1.33	PET hydrolysate	<i>Appl. Catal. B</i> 2022, 307, 121198.
Co-Ni ₂ P/NF	150	1.42	1 M NaOH + 5 g/L PET	<i>Sustainable Energy Fuels</i> 2022,6, 4916-4924.
Mn _{0.1} Ni _{0.9} Co ₂ O _{4-δ} RSFs	50	1.51	1 M KOH + 0.17 M EG	<i>J. Hazard. Mater.</i> 2023, 457, 131743.
B,Co-NiS	10	1.30	1 M KOH + 0.1 M EG	This study
	50	1.322	-	-
	100	1.341	-	-
	150	1.358	-	-
	200	1.374	-	-

Table S3. Calculated charge transfer resistance (R_{ct}) and solution resistance (R_s) (in Ohm, Ω) of electrocatalysts obtained from the Nyquist plot during the EIS experiments.

Catalyst	R_s	R_{ct}
B,Co-NiS	1.59	3.72
Co-NiS	1.64	12.47
B-NiS	1.58	4.53
NiS	1.63	23.26
NF	2.79	50.43

Table S4. A summary of HER properties of B,Co-NiS and state-of-the-art electrocatalysts.

Catalyst	Electrolyte	η_{10} (mV)	Reference
N-doped Ni ₃ S ₂ /NF	1.0 M KOH	155	<i>Adv. Energy Mater.</i> 2018, 8, 1703538.
Mn ₃ (PO ₄) ₂	1.0 M KOH	104	<i>Appl. Catal. B.</i> 2021, 292, 120202.
Reduced NiCo ₂ O ₄	1.0 M KOH	135	<i>J. Am. Chem. Soc.</i> 2018, 140, 13644–13653.
Mo ₂ NiB ₂	1.0 M KOH	160	<i>Small.</i> 2022, 18(6), 2104303.
SrCo _{0.85} Fe _{0.1} P _{0.05} O _{3-δ} nanofilm	1.0 M KOH	110	<i>Adv. Mater.</i> 2018, 30, 1804333.
o-CoSe ₂ P	1.0 M KOH	104	<i>Nat. Commun.</i> 2018, 9, 2533.
N-NiMoO ₄ /NiS ₂	1.0 M KOH	99	<i>Adv. Funct. Mater.</i> 2019, 29, 1805298.
Mn-CoP nanowire@Mn-CoOOH nanosheet	1.0 M KOH	110	<i>Appl. Catal. B.</i> 2021, 292, 120172.
Fe-doped MOF CuCoSe@HCNF	1.0 M KOH	181	<i>Appl. Catal. B.</i> 2021, 293, 120209.
Ni NP Ni–N–C/EG	1.0 M KOH	147	<i>Energy Environ. Sci.</i> , 12 (2019) 149-156.
Fe-doped CoWO ₄	1.0 M KOH	118	<i>J. Mater. Chem. A</i> 2021, 9, 9753-9760
1T-Fe/P-WS ₂ @CC	1.0 M KOH	116	<i>Appl. Catal. B.</i> 2021, 286, 119897.
Ni ₃ S ₂ /VG@NiCo LDHs	1.0 M KOH	120	<i>Chem. Eng. J.</i> 2021, 415, 129048.
NiSe ₂ /Ni ₃ Se ₄ /NF	1.0 M KOH	145	<i>Appl. Catal. B</i> 2022, 303, 120915
MoS ₂ /Co ₉ S ₈ /Ni ₃ S ₂ /Ni	1.0 M KOH	113	<i>J. Am. Chem. Soc.</i> 2019, 141, 10417-10430.
Cu NDs/Ni ₃ S ₂ NTs-CFs	1.0 M KOH	128	<i>J. Am. Chem. Soc.</i> 2018, 140, 610–617.
B,Co-NiS	1.0 M KOH	86	<i>This study</i>